ACS OMEGA

http://pubs.acs.org/journal/acsodf

Article

Novel *Moringa oleifera* Leaves 3D Porous Carbon-Based Electrode Material as a High-Performance EDLC Supercapacitor

Rika Taslim,* Apriwandi Apriwandi, and Erman Taer

Cite This: *ACS Omega* 2022, 7, 36489−36502

Read Online

ACCESS | Metrics & More | Article Recommendations

ABSTRACT: Biomass-based activated carbon has great potential in the use of its versatile 3D porous structures as an excellent electrode material in presenting high conductivity, large porosity, and outstanding stability for electrochemical energy storage devices. In this study, the electrode material develops through a novel consolidated carbon disc binder-free design, which was derived from *Moringa oleifera* leaves (MOLs) for electrochemical double-layer capacitor applications. The carbon discs are prepared in a series of treatments of precarbonized, chemical impregnation of zinc chloride, integrated pyrolysis of N_2 carbonization, and CO_2 physical activation. The physical activation temperatures applied at 650, 750, and 850 °C optimize the precursor potential. By optimizing the 3D hierarchical pore properties of the MOL750, the carbon disc binder-free design demonstrates optimal symmetric supercapacitor performance with a high specific capacitance of 307 F g^{-1} at a current density of 1 A g^{-1} in an aqueous electrolyte solution of 1 M H_2SO_4. Furthermore, the extremely low internal resistance (0.006Ω) of the carbon disc initiated excellent electrical conductivity. The supercapacitors also maintain their high capacitive properties in aqueous electrolyte solutions of 6 M KOH and 1 M Na_2SO_4, respectively. The results show that a novel consolidated carbon disc binder-free design can be obtained from biomass MOLs through a reasonable approach to develop superior electrode materials to enhance high-performance electrochemical energy storage devices.

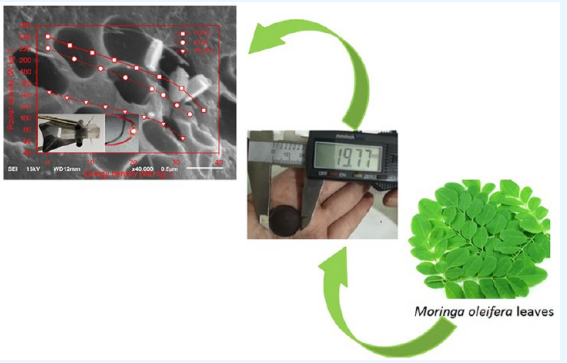

1. INTRODUCTION

The rapid growth of the world's population with the demands for prosperous life management has made the energy crisis the main global challenge. At the end of 2021, energy consumption was 4.5% higher than the previous year[1] and is estimated to increase by more than half in the next 4 years.[2] Moreover, approximately 90% of the total energy demand is obtained from coal, which is nonrenewable. Studies have shown that the use of coal energy sources causes significant problems in the production of CO_2 emissions and greenhouse gas effects, which leads to global warming and climate change.[3] This makes it necessary to develop effective, efficient, and pollution-free green energy technology and renewable energy conversion systems. In the past decade, people have focused on abundant, low-cost, safe, and environmentally friendly renewable energy sources such as wind, ocean waves, solar, and biomass. However, their use was limited due to a relatively low supply of technology and complex supporting components. Several developed countries such as China and the United States have implemented renewable energy technologies as alternative sources of energy.[4] This situation led to the development of energy storage systems and devices with high specifications, good stability, low cost, effectiveness, and efficiency to perfect green energy technologies.[5,6] Among the various energy storage technologies investigated, supercapacitors received much attention due to their outstanding power transmission specifications, fast energy storage, infinite cycle stability, high conductivity, and eco-friendly nature.[7−9] The main key to the superior characteristics of supercapacitor devices is their electrode-based material.[10,11] Various electrode-based materials can produce high and low characteristics of electronic and ionic conductivity. This significantly affects the ability of the electric charge transfusion rate and cyclic resistance of the supercapacitor.[12,13] Therefore, there is a need to design and develop excellent electrode materials for high-performance supercapacitors. In recent years, electrode materials have shown high specifications such as metal oxides, conducting polymers, and carbon materials. The metal oxide materials such as MnO_2, TiO_2, and RuO_2 offer high oxidation states for efficient charge transfer during redox reactions, which generate Faradaic currents and ion intercalation that favor charge storage, high capacity, and conductivity as well as low

Received: July 8, 2022
Accepted: September 29, 2022
Published: October 9, 2022

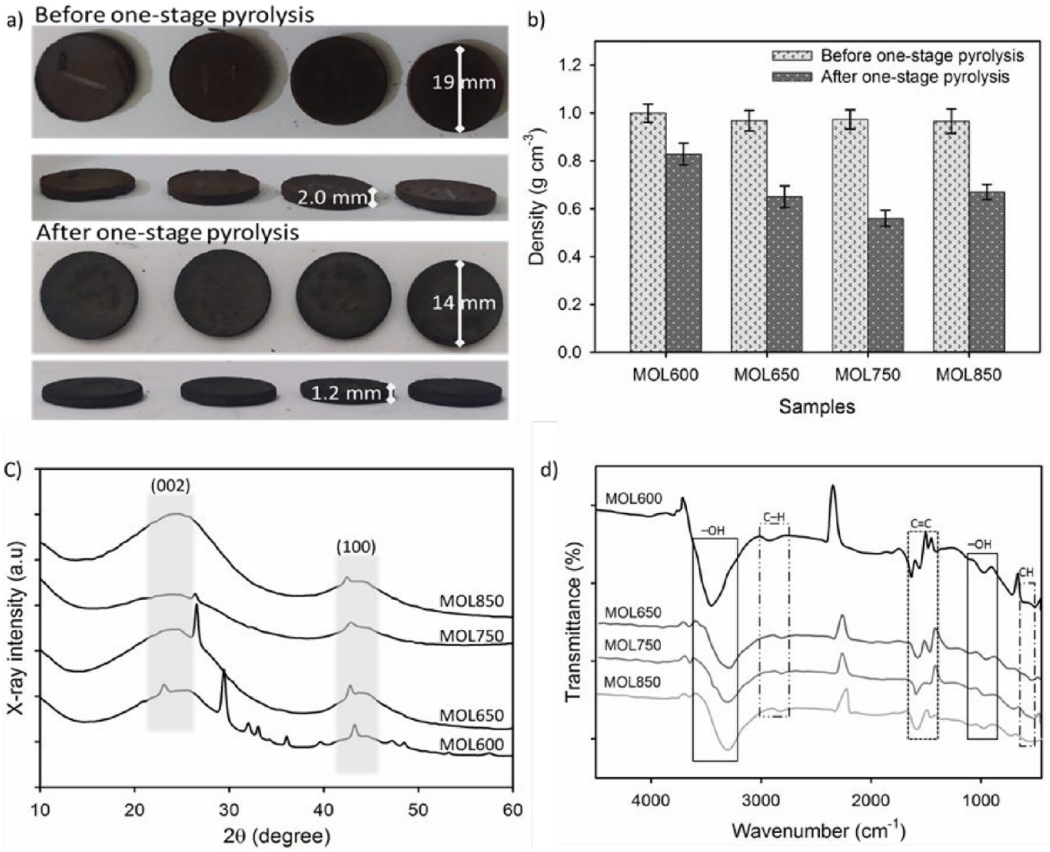

Figure 1. (a) Dimensions of binder-free consolidated discs before and after pyrolysis. (Photograph courtesy of Apriwandi Apriwandi. Copyright 2022). (b) Changes in the density of the carbon discs of MOLs at different temperatures of pyrolysis treatments, (c) XRD pattern of MOLs disc at different pyrolysis temperatures, and (d) FTIR spectrum of the MOLs carbon disc at a wavenumber of 4500−450 cm^{-1}.

toxicity.[14−16] According to Wang et al., the mixed metal oxide material has produced a specific capacitance of 788 F g^{-1} with an energy density of 138 Wh kg^{-1}.[17] Similar results were also confirmed in polymeric materials that produce high energy density.[18] The polymeric materials allow flexible design, which is considered to be more practical, modern, and generally acceptable. The excessive consumption of metal and high-cost polymeric materials with their complicated production methods, low porosity, and corrosive properties significantly increases the risks of mass production and limit their wider application.

Similarly, carbon materials, especially activated carbon, are of greater concern due to their lower production costs, abundant availability, suitable pore structure, and very high porosity properties.[7,19] The biomass-based activated carbon provides a 3D hierarchical pore structure of a combination of micro-, meso-, and macropores that enable the electrode material to produce high energy and power densities simultaneously.[20,21] Moreover, the self-doping of N/O/P on carbon-based biomass also confirmed their high advantage.[22] Activated carbon from the leaves of *Parthenium hysterophorous* (biomass) has shown a 3D porous structure with a high surface area of 4014 m^2 g^{-1} recently, followed by oxygen self-doping.[23] This characteristic has increased the storage capacity of a symmetric supercapacitor to 270 F g^{-1}. The adjustable micro-/macropore ratio of activated carbon from pecan shells can also produce an extraordinary specific capacitance of 447 F g^{-1}[24] and display high electrochemical properties with a surface area of 1,785 m^2 g^{-1}. This showed that the high surface area does not guarantee the high electrochemical properties of the supercapacitor. Some suspicions of tuning micromesopores, heteroatom self-doping, and the natural conductivity of the materials also contribute to the improvement of their electrochemical properties. Similar results were also obtained from other organic-based activated carbon sources such as wood powders,[25] feather finger grass flower,[26] camellia pollen,[27] and peach gum.[28] Meanwhile, the electrode materials of biomass-based activated carbon possessed energy density disproportionately with their power density and electrical/ionic conductivity far from metal oxide materials and conducting polymer due to high porosity, which hinders their practical application. Therefore, it is necessary to design a biomass-based porous carbon with a novel, easy, inexpensive, and approach for environmentally friendly, pollution-free, and high-performance supercapacitors.

Therefore, this study aims to develop a novel electrode material design from *Moringa oleifera* leaves biomass-based consolidated solid carbon discs to increase the storage capacity of symmetric supercapacitor devices. The proposed carbon discs are prepared binder-free, and their treatment consists of precarbonization, chemical impregnation ($ZnCl_2$), integrated pyrolysis of N_2 carbonization, and physical activation of CO_2. The potential for activated carbon precursors was also maximized through different pyrolysis temperatures 650, 750, and 850 °C. Moreover, the carbon discs of MOLs exhibit 3D hierarchical pore properties with oxygen heteroatoms as their additional oxidative property. The optimized carbon disc exhibits a high specific capacitance of 307 F g^{-1} in the 1 M

https://doi.org/10.1021/acsomega.2c04301
ACS Omega 2022, 7, 36489−36502

Table 1. Microcrystalline Parameters and Elemental Status of MOLs Carbon Disc at Different Physical Activation Temperature

	Microcrystalline parameters				Elemental status				
Carbon disc MOLs	d_{002} (Å)	d_{100} (Å)	L_c (Å)	L_a (Å)	C (%)	O (%)	Ca (%)	Cl (%)	Zn (%)
MOL600	3.524	2.077	13.391	22.159	79.45	17.41	2.28	0.87	0.00
MOL650	3.616	2.051	12.297	16.903	85.97	10.49	0.63	0.68	2.24
MOL750	3.698	1.994	7.481	23.866	88.54	8.06	1.11	0.64	1.65
MOL750	3.689	1.993	10.323	18.144	88.91	8.45	1.38	0.60	0.66

H_2SO_4 electrolyte. This showed that the proposed design is a reasonable approach to increase the symmetric storage capacity of pollution-free, low-cost, and high-performance supercapacitors.

2. RESULTS AND DISCUSSION

2.1. Material Analysis. Density analysis is an important aspect for the evaluation of carbon MOLs in form of binder-free consolidated discs. This section shows the analysis of changes in the density of the carbon discs of MOLs at different temperatures of pyrolysis treatments. The precursor powder pressed at a predetermined load was properly compacted at a diameter of ±19.00 mm, a thickness of ±2.00 mm, and a mass of ±0.70 gr (see Figure 1a). The potential precursors of the confirmed MOLs formed a strong/resistant and a fracture-free consolidated disc with a smooth surface. Their biological composition and complex compounds can act as self-adhesives to enable the formation of binder-free strong discs.

A similar case was also stated in a previous study using banana leaves as a precursor.[29] In this study, the average densities of the samples MOL600, MOL650, MOL750, and MOL850 were 0.9990, 0.9680, 0.9730, and 0.9660 g cm^{-3}, respectively. The discs of consolidated MOLs were pyrolyzed at high temperatures, including carbonization in an N_2 gas environment and physical activation in a CO_2 gas environment, and their final process was evaluated for overall dimensional changes.[30] As shown in Figure 1b, the disc density of the consolidated MOLs degraded significantly after the high-temperature pyrolysis process due to a significantly large mass loss. Pyrolysis initiated from 30 to 850 °C for over 10 h significantly degraded the disc dimensions, where their diameter, thickness, and average mass were reduced to ±14.00−13.00 mm, ±1.2−1.0 mm, and 0.2−0.1 gr, respectively. After the pyrolysis process, the MOLs disc density decreased to 0.8280, 0.6500, 0.5600, and 0.6700 g cm^{-3} for samples MOL600, MOL650, MOL750, and MOL850, respectively.

The evaporation of volatile compounds, water content, and decomposition of the biological composition of the precursor during the chemical reaction of $ZnCl_2$ at high-pyrolysis temperature caused the reduction of the density of MOLs discs. Furthermore, the physical appearance of the disc sample is relatively solid black, which indicated a high fixed carbon content. The 42.44% density degradation initiated the formation of a diverse pore framework which is needed as a good electrode material for electrochemical energy storage devices. The different pyrolysis temperatures from 600 to 750 °C affect their respective densities by degrading the MOLs disc density to 32.36%. This is due to the erosion of the carbon framework which causes the expansion of larger pores and initiates the formation of macropores within the micron scale. Upon increasing the pyrolysis temperature from 750 to 850 °C, the density of the disc increased by 16.41% due to excessive erosion of the carbon pore walls. This makes the carbon skeleton unable to maintain the structure above; thus, it collapsed and covered the pores below. However, these results are relatively normal for solid carbon samples.

The material structure of the carbon disc MOLs was evaluated through X-ray diffraction (XRD) and Fourier transform infrared (FTIR) techniques. Figure 1c shows the XRD pattern of disc MOLs at different pyrolysis temperatures of 600, 650, 750, and 850 °C. The carbon discs showed strong broad peaks at angles of 24° and 44° correlated with the (002) and (100) scattering planes, which confirmed the turbostratic carbon structure (JCPDS No. 29-1126, 29-1127).[31] The high-temperature pyrolysis of the precursor MOLs allows the decomposition and rearrangement of the carbon structure to initiate good amorphous behavior.[32]

Furthermore, the properties of the carbon disc structure of MOLs changed during the high-temperature pyrolysis process including carbonization and physical activation. The hkl (002) plane possesses broad peak attenuation from 600 to 850 °C, which significantly reduced the crystalline properties and initiated the formation of abundant micromesoporosity.[33] This property improves the electroactive site of the electrode material in energy storage systems. Meanwhile, the sharp peaks in the sample were significantly reduced from 600 to 850 °C, indicating the presence of a small amount of crystal structure of the compounds $CaCO_3$ and ZnO at angles of 23°, 26°, 29°, 32°, 36°, and 43°.

These compounds are the contribution of organic precursor components and byproducts of their chemical impregnation. The $CaCO_3$ compound is located at angles of 23.165°, 29.255°, 32.050°, and 36.095° (JCPS No. 06-0230) and the ZnO compound in very small amounts at 26.05°−26.395° (JCPDF No. 36-1451).[34,35] The MOLs600 sample that was carbonized at 600 °C produced an XRD pattern containing several $CaCO_3$ crystalline compounds. The application of physical activation in the CO_2 gas environment reduced the $CaCO_3$ compounds as shown in MOLs650, MOLs750, and MOLs850, as described for the EDS technique in Table 1. Moreover, high-temperature pyrolysis obtains carbon discs with a well amorphous structure. Table 1 summarizes the interlayer spacing and microcrystalline dimensions of the MOLs carbon discs at pyrolysis temperatures ranging from 600 to 850 °C. The value of $d_{(002)}$ of MOLs is slightly higher than $d_{(002)}$ of graphite by approximately 3.46%, while $d_{(100)}$ indicates a relatively ideal for amorphous carbon-based biomass as stated in previous studies.[36,37] Furthermore, the microcrystalline dimension (L_c) is closely related to the specific surface area and the active channel on the electrode material, which is often related through empirical equations.[38,39] Based on this empirical equation, L_c showed that the specific surface area inversely, where a low L_c allows the electrode disc to obtain a high surface area. From Table 1, the carbon discs pyrolyzed at 750 °C showed higher surface areas than others.

https://doi.org/10.1021/acsomega.2c04301
ACS Omega 2022, 7, 36489−36502

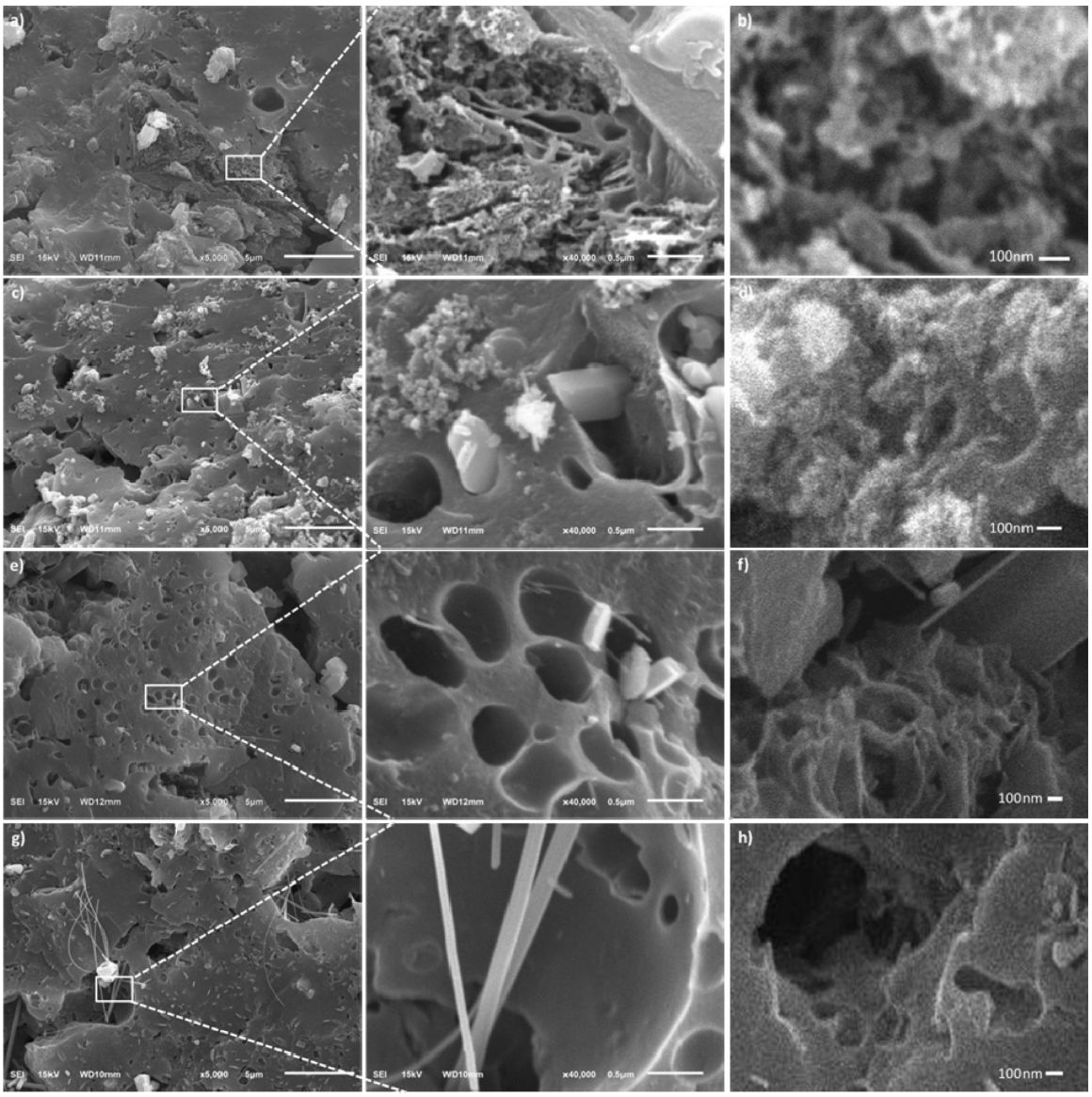

Figure 2. SEM image of (a) MOL600, (b) MOL600 at closer zoom, (c) MOL650, (b) MOL650 at closer zoom, (e) MOL7500, (f) MOL600 at closer zoom, (g) MOL850, and (h) MOL850 at closer zoom.

Figure 1d shows the FTIR spectrum of the carbon disc MOLs at a wavenumber of 4500−450 cm^{-1}. Generally, different pyrolysis temperatures, namely 600, 650, 750, and 850 °C, of the MOLs precursors exhibited stretching vibrations of −OH, C−H, C═C, C−O, CH_2, and C−H aromatics.[40,41] This functional group is considered normal for porous activated carbon based on organic waste. The carbon discs pyrolyzed at 600 °C (carbonization only) showed significant absorption at several wavenumbers compared to higher temperatures. Furthermore, the highest absorption was discovered in the band 3,463−3,309 cm^{-1} due to stretching vibration of −OH,[42] which was also discovered at wavenumber 1,491−1,422 cm^{-1}. The stretching vibration of C−H was indicated at wavenumbers 2,926 and 978 cm^{-1}, while 1,652 cm^{-1} and 1,553 cm^{-1} were the stretching vibrations of C═C. Meanwhile, the absorption band in the range 1,300−1,010 cm^{-1} represents the C−O functional group, while the CH aromatic is located at 770−709 and 540−518 cm^{-1}.[43] The abundance of C and O in this functional group indicates their relatively high content in carbon disc MOLS as shown in Table 1. At higher temperatures, the pyrolysis of MOL650, MOLs750, and MOL850 integrated with the one-stage carbonization and physical activation process showed relatively different absorption patterns. The stretching vibrations of C−O and −OH decreased significantly at MOL650, MOL750, and MOL850, as shown in the absorption bands of 3,400−3,300 and 1,300−1,010 cm^{-1}. This is due to the physical activation in the CO_2 gas environment treatment, maximizing the evaporation process of organic compounds and rearranges the carbon framework, thereby possessing FTIR spectra that are nearly ideal for porous activated carbon. Meanwhile, MOL750 showed the lowest absorption band, followed by the removal of some absorbance, especially on the stretching vibration of C−O and CH aromatic.[40,43] This indicated that the FTIR spectra obtained are the most ideal compared to the others. The presence of a relatively confirmed −OH functional group provides wettability and hydrophilicity properties for the electrode material.[44,45] This property is used as a heteroatom to increase the effect of extra pseudocapacitance in electro-

https://doi.org/10.1021/acsomega.2c04301
ACS Omega 2022, 7, 36489−36502

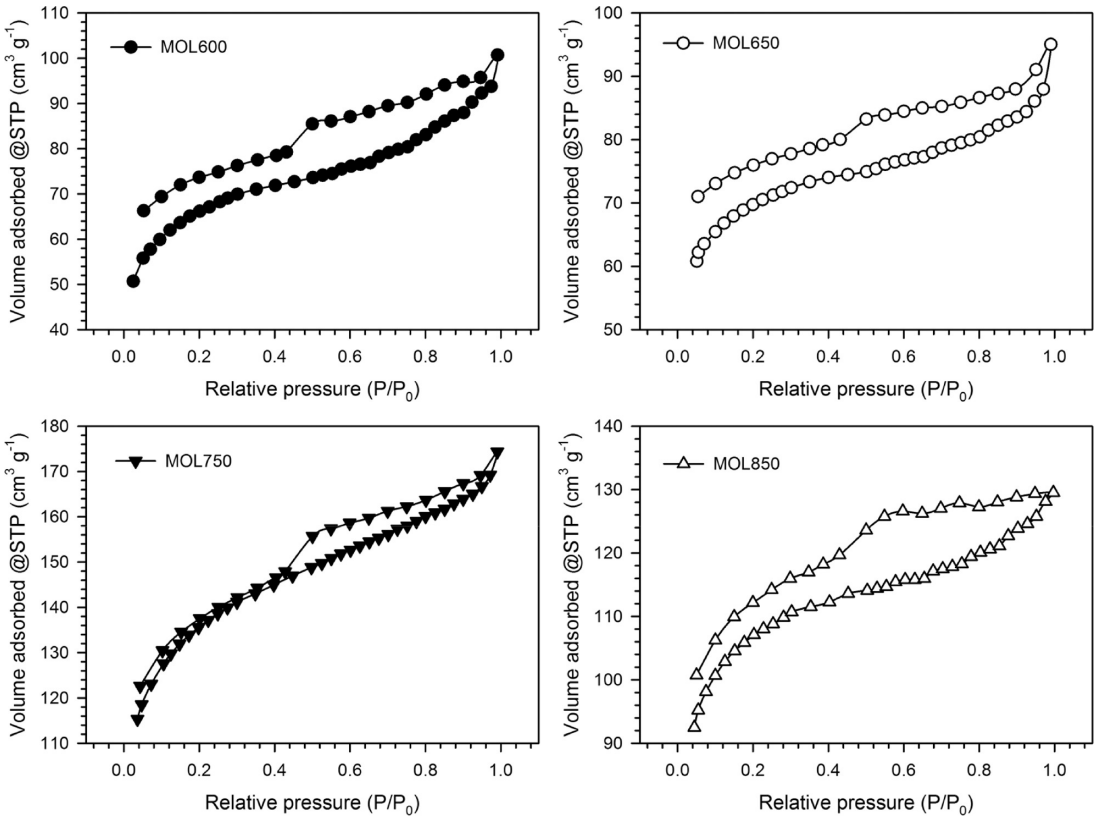

Figure 3. N_2 gas absorption profiles of the MOLs carbon disc.

chemical energy storage devices. Similar results were also shown by EDS and electrochemical property analyses.

Energy-dispersive spectroscopy (EDS) was carried out at a voltage of 15.0 kV within the energy range of 0−20.0 keV to analyze the elements of consolidated carbon discs MOLs that were pyrolyzed at high temperature. Meanwhile, the details elemental status of the carbon disc MOLs is summarized in Table 1. It was shown that carbon (C) is the main component of the highest consolidated disc with approximately 79−89% and oxygen (O) heteroatoms 8−17%, followed by other elements in very small amounts such as potassium (Ca), chlorine (Cl), and zinc (Zn). These results are in line with the previously discussed XRD and FTIR analyses. The carbonization process at 600 °C in the N_2 atmosphere significantly obtained high pure carbon content of 79.45%. This also supported the density analysis where volatile, high water content, complex organic compounds evaporated and degraded. However, as a byproduct, they still leave oxygen in the form of an oxide compound of 17.41%. An increase in the pyrolysis temperature on physical activation using CO_2 increased the elemental carbon by 88.91% at MOL850, while the elemental oxygen is reduced regularly and remains 8.06% at MOLs750. The element Zn appears because the byproduct of chemical impregnation $ZnCl_2$ is not completely evaporated. Meanwhile, the elements Ca and Cl are the contributions of the organic components of the precursor MOLs. The high pure carbon element obtained in the consolidated disc MOLs also allows the electrode material to have high conductivity properties to boost the electrochemical behavior of the supercapacitor.[46] The elemental oxygen can also contribute to self-heteroatoms and provide additional pseudocapacitance to the disc carbon-based electrode material of consolidated MOLs.

The morphological structures of the obtained consolidated MOL carbon discs were reviewed by scanning electron microscopy (SEM) as shown in Figure 2. Binder-free carbon discs pyrolyzed using 600−850 °C different temperatures exhibited a 3D connected pore-rich surface structure. Precursor MOLs that were impregnated with $ZnCl_2$ at 600 °C showed a smooth surface with clear micron-scale pore channels. In the selected area, MOL600 maintains the natural pore structure of MOLs at the nano and micro scale. The pores obtained were dominated by mesopores in the 23−46 nm range and rich in micropores. Furthermore, the $ZnCl_2$ impregnation maximizes the potential of MOLs precursors to provide rich pores through evaporation and gradation of their organic compounds.[47] Figure 2b confirms the mesoporous rich structure in the range of 24 to 49 nm and macropores in the 100 nm scale.

This is useful as an electrolyte reservoir in the electrochemistry of supercapacitors.[48] When the pyrolysis temperature was increased to 650 °C in the CO_2 physical activation process, the surface structure was decorated with holes in the diameter which ranged from 65 nm to 1,261 nm as shown in Figure 2c. The physical activation of CO_2 significantly grows the rich macropores by grinding the carbon skeleton, which is released in form of CO, H_2O, and CO_2.[49] Through a closer zoom, SEM micrographs confirmed the presence of multiple pores connected in 3D hierarchies, where the macropore walls contain mesopores in small numbers. Figure 2d also shows the expansion of the pores toward a larger direction due to high-temperature carbon skeleton grinding compared to Figure 2b. Meanwhile, increasing the pyrolysis temperature to a higher at

https://doi.org/10.1021/acsomega.2c04301
ACS Omega 2022, 7, 36489−36502

750 °C allows MOLs750 to have abundant pores as shown in Figure 2e. The various pore structures obtained range from 500 to 900 nm. Figure 2f shows morphology 3D carbon foam-like interconnected by thin sheetlike struts and open pores with a diameter of several tens of nanometers.

This pore structure significantly contributes to an increase in the amount of ionic charge transfer and electroactive activity in the MOLs of the electrode material.[50] These morphological properties are expected to cause high capacitive properties with greater energy density and power in symmetric supercapacitor devices. Increasing the pyrolysis temperature to 850 °C at MOL850 led to a more severe etching of the carbon matrix, causing considerable pore dilation. Subsequently, the 3D hierarchical porous structure becomes visible as shown in Figure 2g and their magnification selected area. Moreover, MOL850 exhibits a 2D nanofiber structure at a diameter of approximately 73−188 nm, which can lead to the distribution of micropores on their surface. Figure 4h shows the abundant 3D pore morphology connected hierarchically between mesopores and macropores. The analysis showed that increasing the pyrolysis temperature etches the carbon framework giving rise to a 3D porous carbon framework connected to nanoscale 2D nanosheets and nanofibers on MOLs carbon discs. These results indicated that the proposed approach can significantly increase the proportion of hierarchically connected mesopores/macropores in carbon MOLs. Therefore, excellent material properties can be achieved to improve the performance of electrode materials in electrochemical energy storage devices. A more detailed analysis of the pore structure was confirmed through the N_2 adsorption−desorption isotherm characterization. The MOLs carbon discs obtained from the integrated single-stage pyrolysis process at different temperatures of 600−850 °C have type N_2 gas absorption profiles as shown in Figure 3.

The MOL600 carbon discs obtained by carbonization at 600 temperatures have the lowest isotherm curve with mixed types I and IV. This confirmed a low specific surface area of 207 $m^2 g^{-1}$ with micro- and mesopore structures at a ratio of 65.30% and 34.70%, respectively. After the physical activation of CO_2 on MOL650, MOL750, and MOL850 carbon discs, the absorption curve regularly increased. This indicated higher pore properties and specific surface areas that exhibit mixed type I and IV isotherm curves with an H4 type hysteresis loop. It also showed a hierarchical pore combination of micropores and mesopores that are connected.[51,52] Furthermore, the hysteresis loops are open due to the physical structure of the imperfectly developed pores, where their upper surface is smaller than the inner structure and is usually called a bottleneck pore in several studies.[36] Increasing the physical activation temperature from 650 to 750 °C can significantly increase the specific surface area by approximately 2 times from 211 $m^2 g^{-1}$ to 412 $m^2 g^{-1}$. The distribution of their micro and meso surface areas also changes, which affects the electroactive properties of the electrode material. Abundant micropores promote the material by providing rich channels for ion adsorption, which create an electrical layer, while high mesopores contribute to increased barrier-free charge flow.[53,54] Moreover, MOLs750 indicated the presence of a macropore structure in small amounts as shown by an increase in uptake at a relative pressure of $0.95 \leq P/P_0 \leq 1.0$. The macropore structure can also act as a reservoir for electrolyte ions after the confirmation of the electrochemical properties of the supercapacitor,[55] which is in line with the SEM analysis as shown in Figure 2. The complete combination of micro, meso, and macroporous structures in MOL750 is expected to increase the high performance of MOLs precursor-based supercapacitors. An increase in the physical activation temperature to approximately 850 °C in the MOL850 samples exhibited a reduction in N_2 gas uptake with their specific surface area of about 322 $m^2 g^{-1}$. There is a possibility that the overgrowth of the pores prevents their walls from maintaining the carbon skeleton for the top to collapse and cover the pores below. The pore structure parameters are shown in Table 2, while the pore size distribution of the MOLs carbon discs is shown in Figure 4.

Table 2. Porosity Properties of MOLs

Carbon samples	S_{BET} ($m^2 g^{-1}$)	S_{micro} ($m^2 g^{-1}$)	S_{meso} ($m^2 g^{-1}$)	V_{tot} ($cm^3 g^{-1}$)	D_{aver} (nm)
MOL600	207.482	135.500	71.982	0.1558	3.0
MOL650	211.334	165.167	46.167	0.1470	2.7
MOL750	412.196	313.343	98.853	0.2697	2.6
MOL850	322.008	264.035	57.973	0.2004	2.4

The pyrolyzed carbon disc MOLs at different temperatures showed an abundant pore distribution of micropores ($x \leq 2$ nm), which is rich in mesopores ($2 \leq x \leq 18$ nm). Carbonized discs at 600 °C temperatures gave a relatively balanced micromesopores distribution with an average pore diameter of 3.0 nm. The physical activation treatment of CO_2 at a temperature of 650−850 °C also gave abundant micropores, which were dominated by 1.7 nm micropores. In addition, this treatment reduced the mean pore diameter to approximately 2.4 nm as shown in Table 2. These results confirm the formation of a hierarchical pore structure that develops more conducive to charge/ion storage at the electrode/electrolyte interface.[56,57] Furthermore, the physical activation of CO_2 at different temperatures indicated that the hierarchical pore structure varied in the pore ranging from 1.4 to 2.7 nm. The potential for MOLs precursors was also confirmed to obtain 3D hierarchical porous carbon discs.

2.2. Electrochemical Performance Analysis. The electroactive interactions of ionic charge and carbon-based MOLs electrodes were reviewed in detail through cyclic voltammetry (CV) and galvanostatic charge−discharge (GCD) in a two-electrode system in 1 M H_2SO_4 electrolyte. Figure 5a shows the CV curve of the carbon disc MOLs at a scan rate of 1 mV s^{-1}, showing a nearly perfect rectangular shape in a potential window of 0−1 V. This showed the electroactive properties of the normal electrically double-layered carbon disc MOLs. Furthermore, the spike in current density in the potential window of 0.4 to 0.6 V characterizes the additional pseudocapacitance due to the contribution of the heteroatoms as self-doping.[58] It was also discovered that the highest specific capacitance was in the MOL750 carbon disc of 283 F g^{-1}, characterized by the largest rectangular shape, while the lowest capacitance was in MOL600 of 101 F g^{-1}. The CV curve of MOL650 shows a rectangular shape that is larger than MOL600. This indicated that the CO_2 physical activation treatment can significantly increase the capacitive properties of MOL650 discs to approximately 196 F g^{-1}. The physical activation of CO_2 can significantly maximize the impurity evaporation process, thereby initiating the formation of a rich micromesopore structure, which allows more ions to diffuse at the electrolyte/electrode interface.

https://doi.org/10.1021/acsomega.2c04301
ACS Omega 2022, 7, 36489−36502

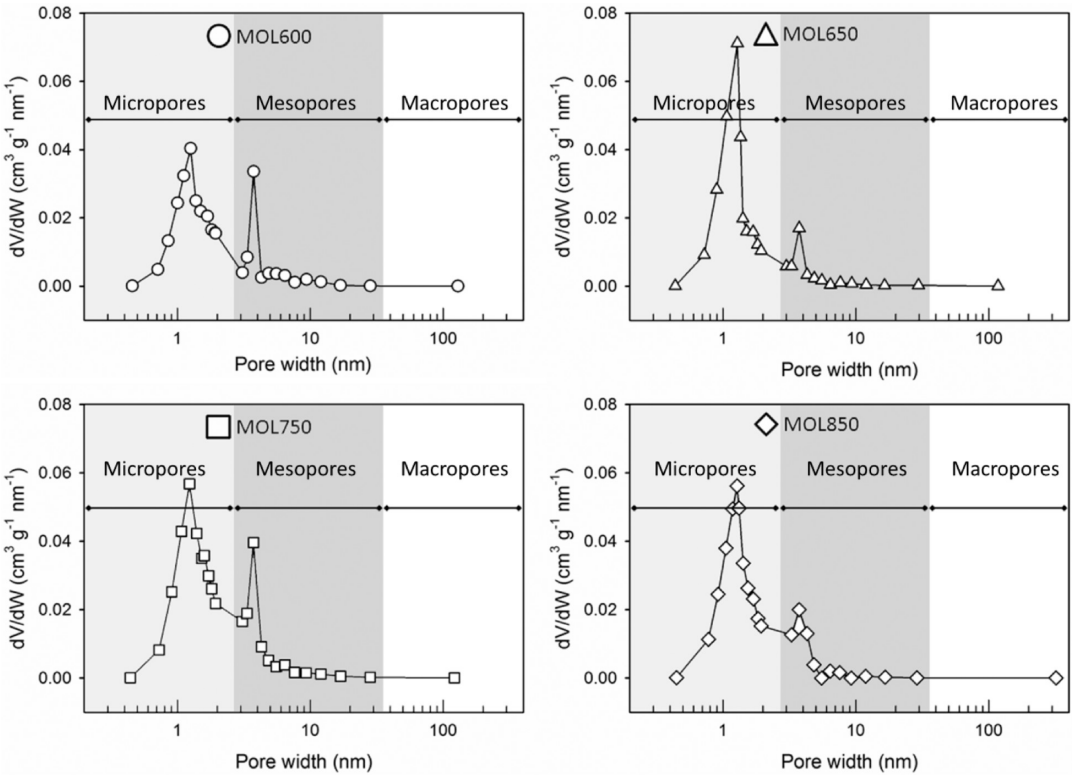

Figure 4. Pore size distribution of the MOLs carbon discs.

The application of a higher activation temperature can maximize the potential of the MOL750 carbon disc, confirming the greatest capacitive properties. This is contributed to their compactly consolidated material structure with a 3D hierarchical structure, followed by an increase in specific surface area. However, the addition of a higher temperature to 850 °C reduces the specific capacitance to 211 F g^{-1}. This is because the intense pore expansion can reduce their surface area as shown in Figure 3 and Table 1, which reduced the electrochemical properties of MOL850. The carbon discs MOL600, MOLs650, MOLs750, and MOL850 were evaluated at various scanning levels as shown in Figure 5b−e to confirm the effect of pores on the performance of the electrode material. It was also discovered that the curve presents a wide rectangular distortion at a scanning speed of 2−5 mV s^{-1}, which shows a good EDLC performance. The pseudocapacitance property was not confirmed at the scanning levels of 2 and 5 mV s^{-1}; therefore, it can be speculated that the electrode material has a weak heteroatom self-doping.[59] Furthermore, at 5 mV s^{-1}, CV curves are obviously different with a significant increase in current followed by an unusual shape indicated due to their relatively low pore structure. This is confirmed similarly to the previous study.[31,60] Moreover, the higher scan rate also confirms the performance of the capacitive properties of carbon MOLs as shown in Figure 5f. The scan rate treatment of 1 to 10 mV s^{-1} significantly reduced the specific capacitance caused by their pore size distribution. However, the MOLs750 carbon disc was able to maintain a specific capacitance of 78% at a scan rate of 10 mV s^{-1}. Figure 6a shows the GCD curves of the disc electrode MOLs at higher physical activation temperatures of 650, 750, and 850 °C in a current density of 1 A g^{-1}. It also showed a distorted isosceles triangle shape, which indicated the nature of the ideal electric double layer. Furthermore, the *iR* drop on the barely visible curve indicates low ion diffusion resistance.[61] Their charge times, which were greater than discharge times, indicated ion degradation due to the presence of self-doping heteroatoms associated with the redox reactions of oxygenated surface functions in the aqueous electrolyte of 1 M H_2SO_4.[22,62] This is supported by the high level of oxygen in the MOLs carbon disc of approximately 8.06−17.41%. The long charge−discharge time of the MOLs disc electrodes characterizes the increase in specific capacitance after the CO_2 physical activation process at temperatures of 650, 750, and 850 °C. The MOLs750 disc electrodes exhibited the longest discharge time, showing that their highest capacitance was 307 F g^{-1}, followed by MOLs850 and MOLs650 of 221 and 156 F g^{-1}, respectively.

This is directly affected by the increase in surface area and accessible pore volume in the carbon disc MOLs, which are required for electrolytic ion charge accumulation and fast unimpeded transport. The physical activation at a high temperature can significantly increase the specific surface area, followed by an increase in the total pore volume and their pore size distribution, which is rich in 3D micromesopores.[54,63] The results also showed that MOLs carbon discs have the highest specific surface area of 433 m^2 g^{-1} with a maximum total volume of 0.244 cm^3 g^{-1}. This allows them to have a high accumulation of electrolyte ions, thereby forming more electroactive layers. The hierarchically connected 3D-rich mesopore structure of MOLs750 confirms their almost unimpeded access to ion transport and the range of diffusion in all directions acting as a reservoir for electrolyte ions.[64] This can significantly improve the capacitive properties of the MOLs carbon electrodes as shown in the MOLs650 to MOLs750 electrodes. An increase in temperature to approximately 850 °C at the MOLs850 carbon disc reduced its capacitive properties as shown by excessive pore expansion. This can cause the pore

https://doi.org/10.1021/acsomega.2c04301
ACS Omega 2022, 7, 36489−36502

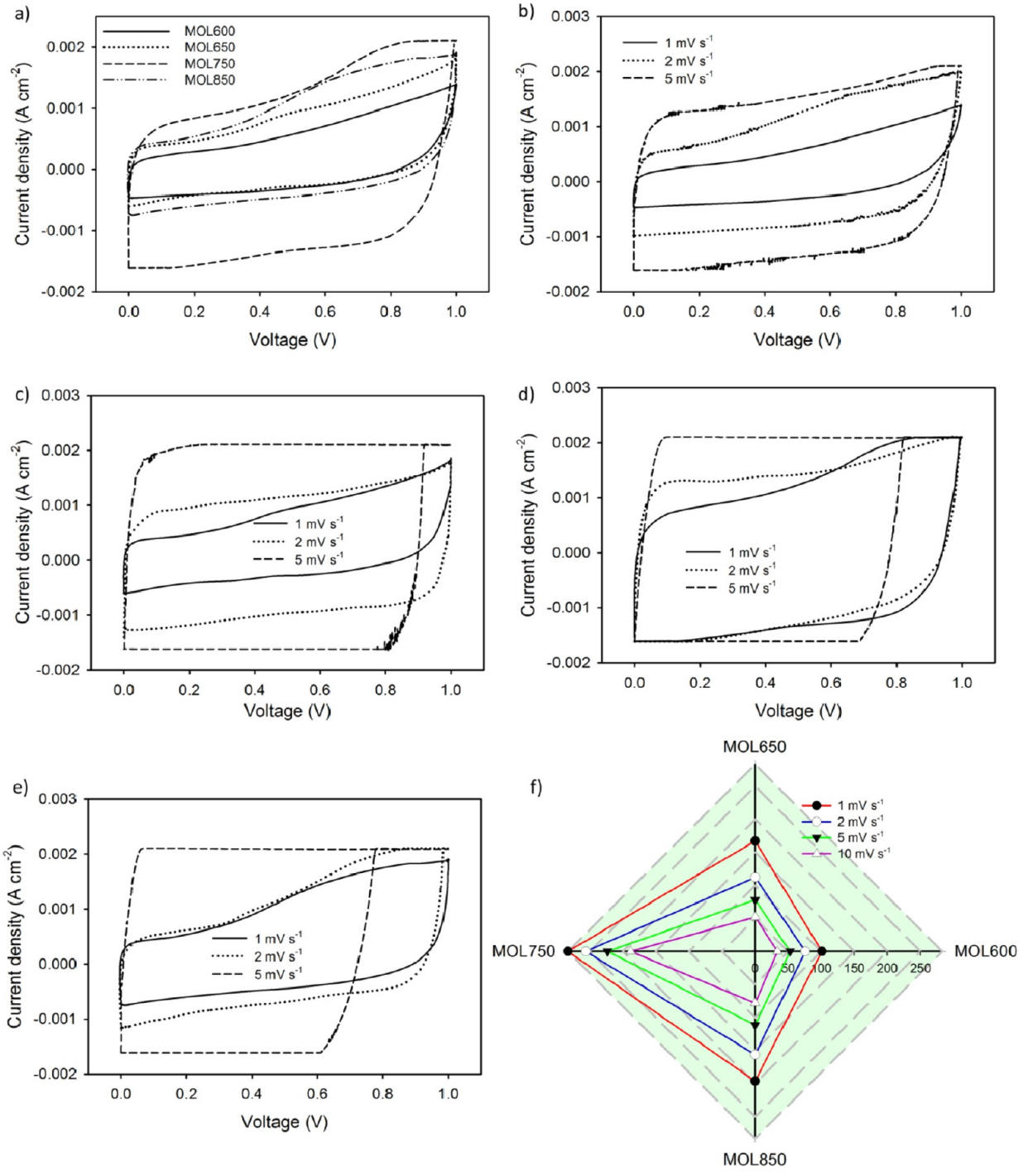

Figure 5. (a) CV curve of the MOLs carbon disc at a scan rate of 1 mV s^{-1}, (b–e) CV curve in different scan rate of MOL600, MOL650, MOL750, and MOL850, and (f) capacitive performance of carbon MOLs at different scan rates in 1 M H_2SO_4 electrolyte.

framework to collapse and cover the hierarchical pores below, which reduced their surface area and pore volume (Table 1).

However, the GCD curve of MOLs750 has the least symmetrical isosceles triangle shape due to the pseudocapacitance effect of oxygen heteroatoms.[17,50] The results obtained from GCD are very similar to SEM, EDS, N_2 adsorption/desorption, and CV images. The Ragone plots confirm the energy and power densities of the MOL650, MOL750, and MOL850 disc electrodes as shown in Figure 6b. Meanwhile, the Ragone plot tends to show that the energy density rises as the physical activation temperature increases at high power density. The MOL650 disc electrode produces an energy density of 25.37 Wh kg^{-1} at a power density of 122.25 W kg^{-1}. An increase in the physical activation temperature on the MOL750 carbon disc gave the most significant energy density of 36.47 Wh kg^{-1} at a power density of 240.73 W kg^{-1} due to the contribution of hierarchically connected 3D micro-mesopores, specific surface area, and self-doping heteroatom. The MOLs850 disc electrode shows an energy density of 27.6876 Wh kg^{-1} with a power density of almost 139.4286 W kg^{-1}. These results indicated that the disc electrode MOLs can produce high properties for electrochemical energy storage

https://doi.org/10.1021/acsomega.2c04301
ACS Omega 2022, 7, 36489–36502

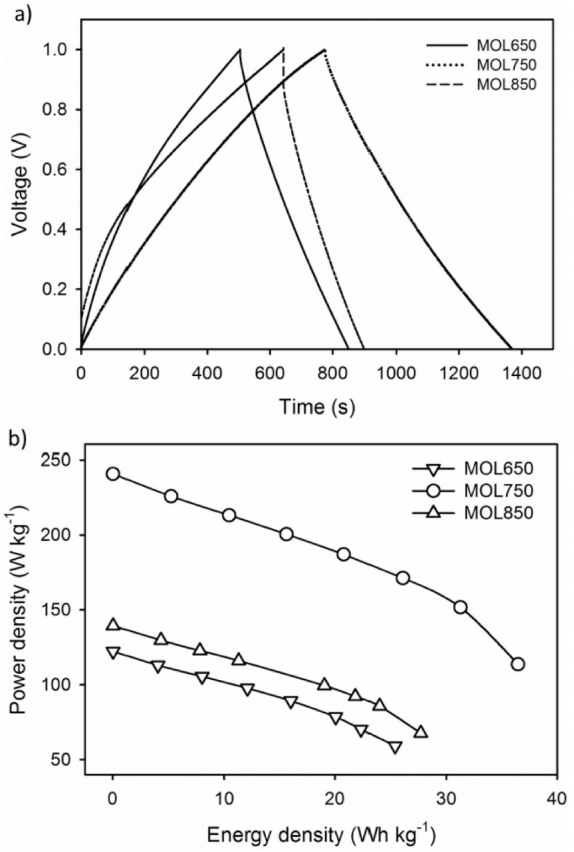

Figure 6. (a) GCD curves of the disc electrode MOLs in 1 M H_2SO_4 electrolyte and (b) Ragone plot of the disc electrode MOLs in 1 M H_2SO_4 electrolyte.

applications. Although the specific surface area of MOL750 is not very high, it can have extraordinary energy density and compete with other studies as summarized in Table 3. This is due to the efficiency of the electrode material designed as solid consolidated carbon discs, which optimized 3D hierarchical pores leading to low internal resistance and high conductivity and producing high electrochemical performance.[26,27]

Table 3. Electrochemical Performance of MOLs Carbon Disc in CV and GCD Techniques

	CV		GCD		
Electrolyte	C_{sp_1} (F g^{-1})	C_{sp_1} (F g^{-1})	E (Wh kg^{-1})	P (W kg^{-1})	R (Ω)
1 M H_2SO_4	283	307	36.47	240.73	0.006
6 M KOH	248	254	33.21	220.75	0.012
1 M Na_2SO_4	202	201	31.59	144.75	0.031

The MOL750 carbon disc electrode was evaluated through different aqueous electrolytes, namely 1 M H_2SO_4, 6 M KOH, and 1 M Na_2SO_4, to confirm the high electrochemical performance. Figure 7a shows the CV curve of the MOLs750 carbon in different aqueous electrolytes. Generally, all aqueous electrolytes showed a distorted rectangular shape, which indicated good EDLC properties. In H_2SO_4 and KOH electrolytes, there was a sudden increase in current density in the voltage range of 0.6−0.8 V. This is closely related to the redox reaction of oxygen heteroatoms under acidic and alkaline aqueous electrolytes that confirms the presence of apparent capacitance. However, it was not discovered in the neutral aqueous electrolyte Na_2SO_4. Based on the magnitude of the formed CV curve, the performance of MOL750 on different electrolytes can be ordered by H_2SO_4 > KOH > Na_2SO_4 with specific capacitances of 283, 248, and 202 F g^{-1}. Improved CV scanning was also applied to MOLs750 in different aqueous electrolytes as shown in Figure 7b−d. All three aqueous electrolytes still produced a distorted rectangular shape, although showing widening toward a parallelogram at scan rates of 2 and 5 mV s^{-1}. This generally exhibited good EDLC performance on acidic, alkaline, and neutral electrolytes. Furthermore, it was discovered that higher scan rates reduced their capacitive properties as shown in Figure 7e. Although specific capacitance was decreased at a scan rate of 10 mV s^{-1} for all electrolytes, they still maintain their capacitive properties of 61−78% with the order H_2SO_4 > KOH > Na_2SO_4. This was significantly contributed by rich mesoporosity >30%, allowing electrolyte ions to diffuse smoothly when their scan is enhanced. Moreover, the contribution of this aqueous electrolyte modification is also reviewed through the GCD technique. Figure 7f depicts the GCD curves of the MOL750 carbon disc electrodes on different electrolytes. It exhibits a nearly ideal isosceles triangular shape, which indicates the normal EDLC properties of an aqueous electrolyte. However, the KOH electrolyte appeared a GCD curve that contained the greatest ion degradation characterized by a charging time, which is significantly different from the discharging time. This is closely related to oxygen heteroatoms with the potential of the evolution of O_2 and H_2 in aqueous electrolyte systems.[65] It was also discovered that the *iR* drop was relatively very low, confirming the high conductivity properties of the MOLs750 precursor as summarized in Table 3.

This phenomenon initiates the high storage capacity of supercapacitors despite their relatively low surface area. Based on the length of the discharge time, the H_2SO_4 electrolyte exhibited the highest specific capacitance, followed by KOH and N_2SO_4 with their capacitive values of 307, 254, and 201 F g^{-1}, respectively. This result is in line with the CV analysis, which also revealed almost similar results. To confirm the practical application,[66] the volumetric capacitance was also evaluated as high as 101.61, 684.07, and 66.53 F cm^{-3} for different electrolytes H_2SO_4, KOH, and Na_2SO_4, respectively. Moreover, modifying the cations and anions in the aqueous electrolyte can affect the electrochemical substance of the supercapacitor, especially at the MOL750 carbon disc electrode. This is due to ionic mobility, ionic hydrated radius, conductivity, and impact on charge/ion exchange as well as diffusion.[67] The small dehydrated sphere of H^+ cations compared to K^+ and Na^+ allows the charge on the cations to produce the greatest molar ionic conductivity and ionic mobility.[68] These characteristics are needed to obtain fast charge transfer and high ion adsorption at the electrolyte/electrode interface. Similarly, the specification of the cationic radius is also closely related to long-term cycle stability for the MOL750 electrode material, as shown in Figure 7e, where the H_2SO_4 electrolyte maintained a specific capacitance of 78%. Anion specifications were also studied in their interactions with the MOL750 disc electrode. The results showed that the OH^- has a narrower hydration ball radius, initiating better conductivity and ionic mobility. Meanwhile, the SO_4^{2-} exhibited a larger hydration ball radius, leading to a decrease in the number of ions accessing the pores and lower electrical double sheet formation.[69] Relative to other anions, SO_4^{2-} ion

https://doi.org/10.1021/acsomega.2c04301
ACS Omega 2022, 7, 36489−36502

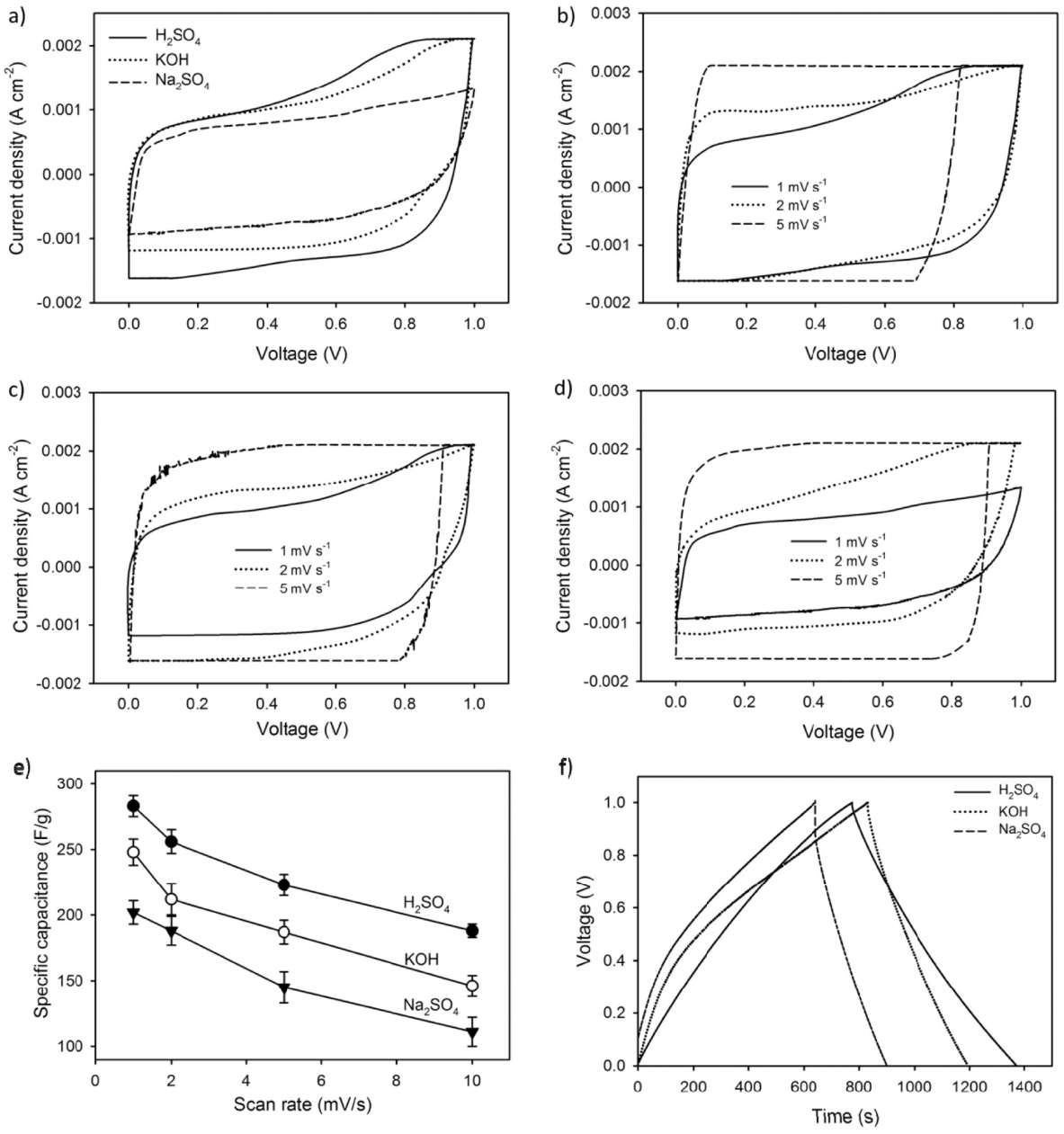

Figure 7. (a) CV curve of the MOLs750 carbon in different aqueous electrolytes, (b–d) Improved CV scanning was also applied to MOLs750 in different aqueous electrolytes, (e) capacitive performance of carbon MOLs in different scan rate in different aqueous electrolytes, and (f) GCD curve of the MOLs750 carbon in different aqueous electrolytes.

has poor conductivity and ion mobility, which makes Na_2SO_4 electrolytes show the lowest capacitive properties compared to H_2SO_4 and KOH electrolytes.

For detailed confirmation, the potential of the MOL750 disc electrode in different aqueous electrolytes was reviewed through the Ragone plot as shown in Figure 8. The H_2SO_4 electrolyte demonstrated the highest performance with an energy density of 36.47 Wh kg^{-1} at a power density of 240.73 W kg^{-1}. Furthermore, 3D hierarchical pore properties with a micro to meso ratio of approximately 3:1 perfectly match the criteria for H^+ anions and SO_4^{2-} cations in aqueous electrolyte H_2SO_4 to possess high energy density in supercapacitor energy storage devices. The alkaline electrolyte KOH also displays an energy density of 33.2047 Wh kg^{-1} at a power density of 220.750 W kg^{-1}, while the neutral electrolyte Na_2SO_4 exhibits an energy density of 31.5964 Wh kg^{-1} at a power density of 144.7541 W kg^{-1}. Moreover, the volumetric energy density is summarized in detail covering 12.07, 10.99, and 10.45 Wh L^{-1} for the different electrolytes H_2SO_4, KOH, and Na_2SO_4, which indicated the great potential of MOL750 electrode as practical applications in electrochemical energy storage devices.[66,70] This result is relatively high compared to previous reports, which are summarized in Table 4

3. CONCLUSION

The green *Moringa oleifera* leaves (MOLs) were converted into a novel consolidated carbon disc-based electrode material through a facile, simple, and environmental approach. The MOLs carbon discs obtained showed a rich 3D hierarchical micromesopore structure decorated nanofibers. Furthermore, oxygen heteroatoms (8.06–17.41%) were confirmed with a

https://doi.org/10.1021/acsomega.2c04301
ACS Omega 2022, 7, 36489–36502

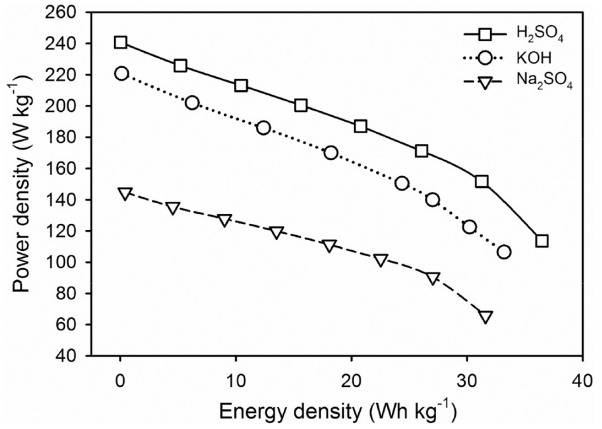

Figure 8. Ragone plot of the disc electrode MOLs in different aqueous electrolytes.

high carbon content of 88.91%. Furthermore, the electrochemical properties of the carbon disc electrodes of MOLs were evaluated in a symmetric supercapacitor system on different aqueous electrolytes. The MOL750 disc electrode showed the best electrochemical properties with a specific capacitance of 307 F g^{-1} on aqueous electrolyte H_2SO_4. Moreover, the MOLs750 discs can maintain their high performance on aqueous electrolytes KOH and Na_2SO_4 with specific capacitances of 254 and 201 F g^{-1} in a current density of 1 A g^{-1}. The design of binder-free consolidated carbon disc MOLs showed their great potential in producing high capacitive properties, lower internal resistance, high conductivity, despite the relatively low surface area of 412.196 m^2 g^{-1}. Therefore, the MOLs can be developed as a novel approach for producing excellent biomass-based electrode material to enhance the performance of energy storage devices in symmetric supercapacitors.

4. EXPERIMENTAL SECTION

4.1. Synthesis of Porous Consolidated Carbon Disc from MOLs. Green *M. oleifera* leaves, hereinafter referred to MOLs, were obtained from a vegetable supplier of the Pekanbaru grand market, separated from the stalks, and cleaned. After the soil and sand elements were removed, the leaves were sun-dried for 2 days and further oven-dried at 110 °C (oven food warmer 10−110C type FW-35) for 35 h until the green precursors turned wilted and brittle. The precursor was converted into powder form through precarbonization, crusher, and sieving. Precarbonization was carried out by preparing 30 g of dried leaf samples in a closed container and placing it in an oven with a temperature of 250 °C (KIRIN Oven 10L KBO 100 M) for 2 h 30 min. The sample obtained from the precarbonization was inserted into the crusher instrument for 24 h. The precursor powder from the crusher was sieved using a 250 mesh (CBN test sieve analysis, cat no. KB-31) to obtain a homogeneous powder, which was chemically activated by zinc chloride impregnated in solution 0.5 mol/L solution. Zinc chloride for analysis was purchased from EMSURE ACS, ISO, Reag. Ph Eur. CAS No. 7646-85-7, EC no. 231-592-0. Subsequently, the dried powder precursor was mixed with $ZnCl_2$ solution on a Digital Lab Thermostatic Hot-Plate instrument (WiseStir Wisd MSH30D) with a rotation rate of 300 rpm at a temperature of 80 °C for 2 h, while the impregnated samples were dried in an oven at 110 °C for 2 days. As a novelty in this study, the carbon powder was converted into a consolidated disc without a binder. For one solid disc sample, 0.7 g of sample powder was pressed through a hydraulic press (Hydraulic Press Bench Type 10T Krisbow KW0500135) at a pressure equal to a mass of 8 tons. 0.7 gr powder samples put in an iron mold resembling a tube with a diameter of 19 mm. The iron mold is pressed using a hydraulic press freely equivalent to ±8.0 tons. A total of 15 monolith solid discs were further put into a vertical furnace (Box Furnace NDT-LB 5, Payun Tech) for high-temperature pyrolysis. The pyrolysis process including carbonization and physical activation was carried out in a single-stage integrated system. This process starts with carbonization in the N_2 gas environment from a temperature of 30 to 600 °C with a gas increase rate of 3 °C/min. The gas environment is replaced with CO_2 as a physical activation stage to a high different temperature of 650, 750, and 850 °C, with an increased rate of 10 °C/min. For comparison, a sample was further prepared at 600 °C without physical activation. Meanwhile, the 3D porous carbon samples obtained were neutralized by soaking in distilled water and HCl in 1 m/L solution. The immersion water was confirmed to be neutral (pH = 7) using a universal pH strip indicator, which was purchased from Merck KGaA, 64271 Darmstadt, Germany. Several labels were made to facilitate the analysis and comparison of materials, as well as electrochemical properties of 3D porous activated carbon-based MOLs. It includes MOL600 as a precursor as well as MOLs650, MOLs750, and MOLs850 from $ZnCl_2$ impregna-

Table 4. Comparison of Electrochemical Performance in Different Carbon Sources

Sources	S_{BET}(m^2 g^{-1})	Electrolyte	Electrode design	C_{sp} (F g^{-1})	E (Wh kg^{-1})	R (Ω)	ref
Wood powders	282.4	6 M KOH	Powder with PTFE	150.1			25
Feather finger grass flower	637.1	6 M KOH	Powder with PTFE	315	18.75		26
Camellia pollen	852	6 M KOH	Powder with PTFE	300	14.3	0.68	27
Sword bean shell	2282	6 M KOH	Powder with PVDF	264	12.5	1.38	44
Foxtail grasses	819	6 M KOH	Powder with PTFE	358	18.2	0.8	53
Calcium D-gluconate	539	1 M H_2SO_4	Powder with PTFE	355	40.5		71
Rubber wood sawdust	2820	1 M H_2SO_4	Powder with PTFE	185	6.93	1.32	72
Kapok flower	1904.1	6 M KOH	Powder with PTFE	286.8		0.79	73
Banana leaves	1459	[BMIM][PF6]	Powder with PVP	190	59		74
Shallot peel	1182.2	1 M H_2SO_4	Solid coin without binder	170.12	16.67	0.031	60
MOLs	412.196	1 M Na_2SO_4	Concolidate disc binder-free	201	31.59	0.031	This work
MOLs	412.196	6 M KOH	Concolidate disc binder-free	254	33.21	0.012	This work
MOLs	412.196	1 M H_2SO_4	Concolidate disc binder-free	307	36.47	0.006	This work

https://doi.org/10.1021/acsomega.2c04301
ACS Omega 2022, 7, 36489−36502

tion and physical activation with different temperatures of 650, 750, and 850 °C.

4.2. Material Characterizations. The initial porosity properties of solid consolidated disc carbon samples were evaluated through density reduction in high temperatures before and after the pyrolysis process. The density was calculated based on measurements of mass using a Labtronics GM-303 analytical balance, thickness, and diameter of the solid carbon monolith pellets using a QRC5 digital caliper.[75] The porosity properties of carbon MOLs were further evaluated through the N_2 gas adsorption/desorption using Quantachrome version 10.01 at a temperature of 77 K in the P/P_0 relative pressure range of 0.00−0.985. The specific surface area was determined with the Breuneur-Emmet-Teller (BET) technique and the pore size distribution was calculated using the density functional theory (DFT) approach. Furthermore, the structure and morphology of activated carbon were reviewed through X-ray diffraction (XRD) and scanning electron microscopy (SEM) methods. X-ray diffraction (XRD) was examined in a CuKα source (λ = 1.54051) at an angle range of 10−60° (Malvern Panalytical's X-ray diffractometers), while interlayer spacing was calculated using Braggs law and lattice parameters (L_c and L_a), which were determined by the Debye−Scherrer equation.[36,37] Similarly, scanning electron microscopy (SEM) was reviewed at a voltage of 15 kV in the energy range 0−20 keV using a JEOL-JSM6510LA instrument. The elemental status of MOLs was also reviewed through the energy-dispersive spectroscopy method (JEOL-JSM-6510-LA instrument).

4.3. Measurement of Electrochemical Properties. The working electrodes were prepared in a two-system configuration similar to a binder-free two solid disc carbon MOLs with a loading mass of approximately ±10.0 mg. The carbon disc obtained from pyrolysis was polished using P1200 polishing paper to obtain carbon discs with diameters and thicknesses of ±8 and 0.19 mm, respectively. Here, two carbon discs as binder-free electrodes were prepared with a diameter of ±8.0 mm with a thickness of 0.19 mm. They were separated by an organic separator made from eggshell membranes. As a support for the electrode, the cell body was made in a rectangular geometry with a hole of ±9.0 mm diameter in the middle. The current collector was prepared from 0.2 mm stainless steel, and an aqueous electrolyte consisting of 1 M H_2SO_4, 6 M KOH, and 1 M Na_2SO_4 was selected. Subsequently, the electrochemical properties were reviewed using cyclic voltammetry technique with CV, RAD-ER 5841, calibrated error ±6.0% in a potential window range of 0.0−1.0 V at different scanning rates of 1, 2, 5, and 10 mV s^{-1}. Specific capacitance, energy and power densities, and internal resistance were further evaluated through the galvanostatic charge−discharge technique using GCD, RAD-ER 2018 at a constant current density of 1.0 A g^{-1} based on the standard equation[76]

$$C_{sp} = \frac{I \cdot \Delta t}{m \cdot \Delta V}$$

$$E_{sp} = \int IV \, dt$$

$$P_{sp} = \frac{E_{sp}}{t}$$

where C_{sp} (F g^{-1}) is the specific capacitance, I (A) is the current, Δt (s) is the discharge time, m (g) is the mass working electrode, ΔV (V) is the voltage discharge, E_{sp} (Wh kg^{-1}) is the energy density, and P_{sp} is the power density (W kg^{-1}).

AUTHOR INFORMATION

Corresponding Author

Rika Taslim − *Department of Industrial Engineering, State Islamic University of Sultan Syarif Kasim, Pekanbaru 28293, Indonesia;* orcid.org/0000-0003-1946-1299; Email: rikataslim@gmail.com

Authors

Apriwandi Apriwandi − *Department of Physics, Faculty of Mathematics and Natural Sciences, University of Riau, Pekanbaru 28293, Indonesia*

Erman Taer − *Department of Physics, Faculty of Mathematics and Natural Sciences, University of Riau, Pekanbaru 28293, Indonesia;* orcid.org/0000-0003-4463-8252

Complete contact information is available at: https://pubs.acs.org/10.1021/acsomega.2c04301

Notes

The authors declare no competing financial interest.

ACKNOWLEDGMENTS

The research was financially supported by the second years Project of Word Class Research (WCR) in Kementerian Pendidikan, Kebudayaan, Riset, dan Teknologi, Republic of Indonesia, with the title "High energy and power densities of supercapacitor for the optimization of electrode supply process". This study also was funded by collaborative grants between universities, State Islamic University of Sultan Syarif Kasim Riau, through Contract No. 873/Un.04/L.1/TL.01/03/2022

REFERENCES

(1) International Energy Agency. *Global Energy Review 2021*, 2021.
(2) BP. *Statistical Review of World Energy*, 2021, Vol. *70*.
(3) BPSTATS. *Review of World Energy Statistical Review of World*, 68th ed.; BP, 2019.
(4) REN21. *Renewables 2021 Global Status Report*, 2021.
(5) Burke, A. Ultracapacitors: Why, How, and Where Is the Technology. *J. Power Sources* **2000**, *91* (1), 37−50.
(6) Li, X.; Zhang, J.; Liu, B.; Su, Z. A Critical Review on the Application and Recent Developments of Post-Modified Biochar in Supercapacitors. *J. Clean. Prod.* **2021**, *310* (April), 127428.
(7) Zhang, W.; Cheng, R. R.; Bi, H. H.; Lu, Y. H.; Ma, L. B.; He, X. J. A Review of Porous Carbons Produced by Template Methods for Supercapacitor Applications. *Xinxing Tan Cailiao/New Carbon Mater.* **2021**, *36* (1), 69−81.
(8) Miller, E. E.; Hua, Y.; Tezel, F. H. Materials for Energy Storage: Review of Electrode Materials and Methods of Increasing Capacitance for Supercapacitors. *J. Energy Storage* **2018**, *20* (February), 30−40.
(9) Taer, E.; Taslim, R. Brief Review: Preparation Techniques of Biomass Based Activated Carbon Monolith Electrode for Supercapacitor Applications. *AIP Conf. Proc.* **2018**, *1927*, 020004.
(10) González, A.; Goikolea, E.; Barrena, J. A.; Mysyk, R. Review on Supercapacitors: Technologies and Materials. *Renew. Sustain. Energy Rev.* **2016**, *58*, 1189−1206.
(11) Wang, G.; Zhang, L.; Zhang, J. A Review of Electrode Materials for Electrochemical Supercapacitors. *Chem. Soc. Rev.* **2012**, *41* (2), 797−828.
(12) Dessie, Y.; Tadesse, S.; Eswaramoorthy, R.; Abebe, B. Recent Developments in Manganese Oxide Based Nanomaterials with

https://doi.org/10.1021/acsomega.2c04301
ACS Omega 2022, 7, 36489−36502

Oxygen Reduction Reaction Functionalities for Energy Conversion and Storage Applications: A Review. *J. Sci. Adv. Mater. Devices* **2019**, *4* (3), 353−369.
(13) Soltani, S.; Khanian, N.; Choong, T. S. Y.; Rashid, U. Recent Progress in the Design and Synthesis of Nanofibers with Diverse Synthetic Methodologies: Characterization and Potential Applications. *New J. Chem.* **2020**, *44* (23), 9581−9606.
(14) Zhang, Q. Z.; Zhang, D.; Miao, Z. C.; Zhang, X. L.; Chou, S. L. Research Progress in MnO2-Carbon Based Supercapacitor Electrode Materials. *Small* **2018**, *14* (24), 1−15.
(15) Arunachalam, R.; Prataap, R. K. V.; Pavul Raj, R.; Mohan, S.; Vijayakumar, J.; Péter, L.; Al Ahmad, M. Pulse Electrodeposited RuO2 Electrodes for High-Performance Supercapacitor Applications. *Surf. Eng.* **2019**, *35* (2), 102−108.
(16) Li, J.; Hu, H.; Li, H.; Yao, C. Recent Developments in Electrochemical Sensors Based on Nanomaterials for Determining Glucose and Its Byproduct H2O2. *J. Mater. Sci.* **2017**, *52* (17), 10455−10469.
(17) Wang, J.; Zheng, F.; Yu, Y.; Hu, P.; Li, M.; Wang, J.; Fu, J.; Zhen, Q.; Bashir, S.; Liu, J. L. Symmetric Supercapacitors Composed of Ternary Metal Oxides (NiO/V2O5/MnO2) Nanoribbon Electrodes with High Energy Storage Performance. *Chem. Eng. J.* **2021**, *426* (August), 131804.
(18) Zang, S.; Jiang, J.; An, Y.; Li, Z.; Guo, H.; Sun, Y.; Dou, H.; Zhang, X. A Novel Porous Organic Polymer-Derived Hierarchical Carbon for Supercapacitors with Ultrahigh Energy Density and Durability. *J. Electroanal. Chem.* **2020**, *876*, 114723.
(19) Majid, S.; Ali, A. S. G.; Cao, W. Q.; Reza, R.; Ge, Q. Biomass-Derived Porous Carbons as Supercapacitor Electrodes-A Review. *New Carbon Mater.* **2021**, *36* (3), 546−572.
(20) Saini, S.; Chand, P.; Joshi, A. Biomass Derived Carbon for Supercapacitor Applications: Review. *J. Energy Storage* **2021**, *39* (April), 102646.
(21) Li, Z.; Guo, D.; Liu, Y.; Wang, H.; Wang, L. Recent Advances and Challenges in Biomass-Derived Porous Carbon Nanomaterials for Supercapacitors. *Chem. Eng. J.* **2020**, *397* (October), 125418.
(22) Gopalakrishnan, A.; Badhulika, S. Effect of Self-Doped Heteroatoms on the Performance of Biomass-Derived Carbon for Supercapacitor Applications. *J. Power Sources* **2020**, *480* (August), 228830.
(23) Aruchamy, K.; Dharmalingam, K.; Lee, C. W.; Mondal, D.; Sanna Kotrappanavar, N. Creating Ultrahigh Surface Area Functional Carbon from Biomass for High Performance Supercapacitor and Facile Removal of Emerging Pollutants. *Chem. Eng. J.* **2022**, *427* (April), 131477.
(24) Zhang, Y.; Wu, C.; Dai, S.; Liu, L.; Zhang, H.; Shen, W.; Sun, W.; Ming Li, C. Rationally Tuning Ratio of Micro- to Meso-Pores of Biomass-Derived Ultrathin Carbon Sheets toward Supercapacitors with High Energy and High Power Density. *J. Colloid Interface Sci.* **2022**, *606*, 817−825.
(25) Wang, C.; Wang, H.; Dang, B.; Wang, Z.; Shen, X.; Li, C.; Sun, Q. Ultrahigh Yield of Nitrogen Doped Porous Carbon from Biomass Waste for Supercapacitor. *Renew. Energy* **2020**, *156*, 370−376.
(26) Senthil, R. A.; Yang, V.; Pan, J.; Sun, Y. A Green and Economical Approach to Derive Biomass Porous Carbon from Freely Available Feather Finger Grass Flower for Advanced Symmetric Supercapacitors. *J. Energy Storage* **2021**, *35* (January), 102287.
(27) Cao, L.; Li, H.; Xu, Z.; Zhang, H.; Ding, L.; Wang, S.; Zhang, G.; Hou, H.; Xu, W.; Yang, F.; Jiang, S. Comparison of the Heteroatoms-Doped Biomass-Derived Carbon Prepared by One-Step Nitrogen-Containing Activator for High Performance Supercapacitor. *Diam. Relat. Mater.* **2021**, *114* (November), 108316.
(28) Wang, L.; Li, X.; Huang, X.; Han, S.; Jiang, J. Activated Green Resources to Synthesize N, P Co-Doped O-Rich Hierarchical Interconnected Porous Carbon for High-Performance Supercapacitors. *J. Alloys Compd.* **2022**, *891*, 161908.
(29) Apriwandi, A.; Taer, E.; Farma, R.; Setiadi, R. N.; Amiruddin, E. A Facile Approach of Micro-Mesopores Structure Binder-Free Coin/Monolith Solid Design Activated Carbon for Electrode Supercapacitor. *J. Energy Storage* **2021**, *40* (June), 102823.
(30) Farma, R.; Deraman, M.; Omar, R.; Awitdrus; Ishak, M. M.; Taer, E.; Talib, I. A. Binderless Composite Electrode Monolith from Carbon Nanotube and Biomass Carbon Activated by KOH and CO2 Gas for Supercapacitor. *AIP Conf. Proc.* **2011**, *1415*, 180−184.
(31) Taer, E.; Apriwandi; Dalimunthe, B. K. L.; Taslim, R. A Rod-like Mesoporous Carbon Derived from Agro-Industrial Cassava Petiole Waste for Supercapacitor Application. *J. Chem. Technol. Biotechnol.* **2021**, *96* (3), 662−671.
(32) Martínez-Casillas, D. C.; Mascorro-Gutiérrez, I.; Arreola-Ramos, C. E.; Villafán-Vidales, H. I.; Arancibia-Bulnes, C. A.; Ramos-Sánchez, V. H.; Cuentas-Gallegos, A. K. A Sustainable Approach to Produce Activated Carbons from Pecan Nutshell Waste for Environmentally Friendly Supercapacitors. *Carbon N. Y.* **2019**, *148*, 403−412.
(33) Wei, H.; Wang, H.; Li, A.; Li, H.; Cui, D.; Dong, M.; Lin, J.; Fan, J.; Zhang, J.; Hou, H.; Shi, Y.; Zhou, D.; Guo, Z. Advanced Porous Hierarchical Activated Carbon Derived from Agricultural Wastes toward High Performance Supercapacitors. *J. Alloys Compd.* **2020**, *820*, 153111.
(34) Achour, A.; Arman, A.; Islam, M.; Zavarian, A. A.; Al-zubaidi, A. B.; Szade, J. Synthesis and Characterization of Porous CaCO3Micro/Nano-Particles. *Eur. Phys. J. PLUS* **2017**, *132*, 267.
(35) Jose, A.; Devi, K. R. S.; Pinheiro, D.; Lakshmi, S. Electrochemical Synthesis, Photodegradation and Antibacterial Properties of PEG Capped Zinc Oxide Nanoparticles. *J. Photochem. Photobiol. B Biol.* **2018**, *187*, 25−34.
(36) Ayinla, R. T.; Dennis, J. O.; Zaid, H. M.; Sanusi, Y. K.; Usman, F.; Adebayo, L. L. A Review of Technical Advances of Recent Palm Bio-Waste Conversion to Activated Carbon for Energy Storage. *J. Clean. Prod.* **2019**, *229*, 1427−1442.
(37) Yaya, A.; Agyei-Tuffour, B.; Dodoo-Arhin, D.; Nyankson, E.; Annan, E.; Konadu, D. S.; Sinayobye, E.; Baryeh, E. a.; Ewels, C. P. Layered Nanomaterials- A Review. *Glob. J. Eng. Des. Technol.* **2012**, *1* (2), 32−41.
(38) Deraman, M.; Daik, R.; Soltaninejad, S.; Nor, N. S. M.; Awitdrus; Farma, R.; Mamat, N. F.; Basri, N. H.; Othman, M. A. R. A New Empirical Equation for Estimating Specific Surface Area of Supercapacitor Carbon Electrode from X-Ray Diffraction. *Adv. Mater. Res.* **2015**, *1108*, 1−7.
(39) Kumar, K.; Saxena, R. K.; Kothari, R.; Suri, D. K.; Kaushik, N. K.; Bohra, J. N. Correlation between Adsorption and X-Ray Diffraction Studies on Viscose Rayon Based Activated Carbon Cloth. *Carbon N. Y.* **1997**, *35* (12), 1842−1844.
(40) Riyanto, C.; Kristen, U.; Wacana, S.; Ampri, M. S.; Martono, Y.; Kristen, U.; Wacana, S. Synthesis and Characterization of Nano Activated Carbon from Annatto Peels (Bixa Orellana L.) Viewed from Temperature Activation and Impregnation Ratio of H3PO4. *J. Sci. data Anal.* **2020**, *1* (1), 44−50.
(41) Salakhum, S.; Yutthalekha, T.; Chareonpanich, M.; Limtrakul, J.; Wattanakit, C. Synthesis of Hierarchical Faujasite Nanosheets from Corn Cob Ash-Derived Nanosilica as Efficient Catalysts for Hydrogenation of Lignin-Derived Alkylphenols. *Microporous Mesoporous Mater.* **2018**, *258*, 141−150.
(42) Pourhosseini, S. E. M.; Norouzi, O.; Naderi, H. R. Study of Micro/Macro Ordered Porous Carbon with Olive-Shaped Structure Derived from Cladophora Glomerata Macroalgae as Efficient Working Electrodes of Supercapacitors. *Biomass and Bioenergy* **2017**, *107* (October), 287−298.
(43) Li, J.; Zou, Y.; Xiang, C.; Xu, F.; Sun, L.; Li, B.; Zhang, J. Osmanthus Fragrans-Derived N-Doped Porous Carbon for Supercapacitor Applications. *J. Energy Storage* **2021**, *42*, 103017.
(44) Chen, T.; Luo, L.; Luo, L.; Deng, J.; Wu, X.; Fan, M.; Du, G.; Zhao, W. High Energy Density Supercapacitors with Hierarchical Nitrogen-Doped Porous Carbon as Active Material Obtained from Bio-Waste. *Renew. Energy* **2021**, *175*, 760−769.
(45) Liang, Y.; Lu, Y.; Xiao, G.; Zhang, J.; Chi, H.; Dong, Y. Hierarchical Porous Nitrogen-Doped Carbon Microspheres after

https://doi.org/10.1021/acsomega.2c04301
ACS Omega 2022, 7, 36489−36502

Thermal Rearrangement as High Performance Electrode Materials for Supercapacitors. *Appl. Surf. Sci.* **2020**, *529*, 147141.
(46) Bhat, V. S.; Kanagavalli, P.; Sriram, G.; B, R. P.; John, N. S.; Veerapandian, M.; Kurkuri, M.; Hegde, G. Low Cost, Catalyst Free, High Performance Supercapacitors Based on Porous Nano Carbon Derived from Agriculture Waste. *J. Energy Storage* **2020**, *32* (August), 101829.
(47) Márquez-Montesino, F.; Torres-Figueredo, N.; Lemus-Santana, A.; Trejo, F. Activated Carbon by Potassium Carbonate Activation from Pine Sawdust (Pinus Montezumae Lamb.). *Chem. Eng. Technol.* **2020**, *43* (9), 1716−1725.
(48) Zhang, Y.; Yu, S.; Lou, G.; Shen, Y.; Chen, H.; Shen, Z.; Zhao, S.; Zhang, J.; Chai, S.; Zou, Q. Review of Macroporous Materials as Electrochemical Supercapacitor Electrodes. *J. Mater. Sci.* **2017**, *52* (19), 11201−11228.
(49) Boujibar, O.; Ghamouss, F.; Ghosh, A.; Achak, O.; Chafik, T. Efficient CO2 Capture by Ultra-High Microporous Activated Carbon Made from Natural Coal. *Chem. Eng. Technol.* **2021**, *44* (1), 148−155.
(50) Yakaboylu, G. A.; Jiang, C.; Yumak, T.; Zondlo, J. W.; Wang, J.; Sabolsky, E. M. Engineered Hierarchical Porous Carbons for Supercapacitor Applications through Chemical Pretreatment and Activation of Biomass Precursors. *Renew. Energy* **2021**, *163*, 276−287.
(51) Sing, K. S. W. Reporting Physisorption Data for Gas/Solid Systems with Special Reference to the Determination of Surface Area and Porosity. *Pure Appl. Chem.* **1982**, *54* (11), 2201−2218.
(52) Zheng, G.; Huang, Z.; Liu, Z. Cooperative Utilization of Beet Pulp and Industrial Waste Fly Ash to Produce N/P/O Self-Co-Doped Hierarchically Porous Carbons for High-Performance Supercapacitors. *J. Power Sources* **2021**, *482* (September), 228935.
(53) Liang, X.; Liu, R.; Wu, X. Biomass Waste Derived Functionalized Hierarchical Porous Carbon with High Gravimetric and Volumetric Capacitances for Supercapacitors. *Microporous Mesoporous Mater.* **2021**, *310* (September), 110659.
(54) Zhang, X.; Liu, B.; Yan, X.; Zhao, X.; Zhang, Y.; Wei, Y.; Cao, Q. Design and Structure Optimization of 3D Porous Graphitic Carbon Nanosheets for High-Performance Supercapacitor. *Microporous Mesoporous Mater.* **2020**, *309* (August), 110580.
(55) Wang, Y.; Qiao, M.; Mamat, X. Nitrogen-Doped Macro-Meso-Micro Hierarchical Ordered Porous Carbon Derived from ZIF-8 for Boosting Supercapacitor Performance. *Appl. Surf. Sci.* **2021**, *540* (P1), 148352.
(56) Wu, J.; Xia, M.; Zhang, X.; Chen, Y.; Sun, F.; Wang, X.; Yang, H.; Chen, H. Hierarchical Porous Carbon Derived from Wood Tar Using Crab as the Template: Performance on Supercapacitor. *J. Power Sources* **2020**, *455* (February), 227982.
(57) Yang, V.; Senthil, R. A.; Pan, J.; Kumar, T. R.; Sun, Y.; Liu, X. Hierarchical Porous Carbon Derived from Jujube Fruits as Sustainable and Ultrahigh Capacitance Material for Advanced Supercapacitors. *J. Colloid Interface Sci.* **2020**, *579*, 347−356.
(58) Huo, S.; Zhang, X.; Liang, B.; Zhao, Y.; Li, K. Synthesis of Interconnected Hierarchically Porous Carbon Networks with Excellent Diffusion Ability Based on NaNO3 Crystal-Assisted Strategy for High Performance Supercapacitors. *J. Power Sources* **2020**, *450* (December), 227612.
(59) Sekhon, S. S.; Park, J. S. Biomass-Derived N-Doped Porous Carbon Nanosheets for Energy Technologies. *Chem. Eng. J.* **2021**, *425* (December), 129017.
(60) Taer, E.; Apriwandi, A.; Rama, D. Solid Coin-like Design Activated Carbon Nanospheres Derived from Shallot Peel Precursor for Boosting Supercapacitor Performance. *J. Mater. Res. Technol.* **2021**, *15*, 1732−1741.
(61) Hor, A. A.; Hashmi, S. A. Optimization of Hierarchical Porous Carbon Derived from a Biomass Pollen-Cone as High-Performance Electrodes for Supercapacitors. *Electrochim. Acta* **2020**, *356*, 136826.
(62) Liu, H.; Liu, R.; Xu, C.; Ren, Y.; Tang, D.; Zhang, C.; Li, F.; Wei, X.; Zhang, R. Oxygen-Nitrogen-Sulfur Self-Doping Hierarchical Porous Carbon Derived from Lotus Leaves for High-Performance Supercapacitor Electrodes. *J. Power Sources* **2020**, *479*, 228799.
(63) Zhang, Q.; Han, K.; Li, S.; Li, M.; Li, J.; Ren, K. Synthesis of Garlic Skin-Derived 3D Hierarchical Porous Carbon for High-Performance Supercapacitors. *Nanoscale* **2018**, *10* (5), 2427−2437.
(64) Liu, H.; Gao, F.; Fan, Q.; Wei, C.; Ma, C.; Shi, J. Preparation of Novel 3D Hierarchical Porous Carbon Membrane as Flexible Free-Standing Electrode for Supercapacitors. *J. Electroanal. Chem.* **2020**, *873*, 114409.
(65) Taer, E.; Taslim, R.; Apriwandi, A. Ultrahigh Capacitive Supercapacitor Derived from Self-Oxygen Doped Biomass-Based 3D Porous Carbon Sources. *ChemNanoMat* **2022**, *8* (2), No. e202100388.
(66) Wang, Q.; Yan, J.; Fan, Z. Carbon Materials for High Volumetric Performance Supercapacitors: Design, Progress, Challenges and Opportunities. *Energy Environ. Sci.* **2016**, *9*, 729−762.
(67) Sajjad, M.; Khan, M. I.; Cheng, F.; Lu, W. A Review on Selection Criteria of Aqueous Electrolytes Performance Evaluation for Advanced Asymmetric Supercapacitors. *J. Energy Storage* **2021**, *40*, 102729.
(68) Aldama, I.; Barranco, V.; Kunowsky, M.; Ibañez, J.; Rojo, J. M. Contribution of Cations and Anions of Aqueous Electrolytes to the Charge Stored at the Electric Electrolyte/Electrode Interface of Carbon-Based Supercapacitors. *J. Phys. Chem. C* **2017**, *121* (22), 12053−12062.
(69) Selvaraj, A. R.; Muthusamy, A.; In-ho-Cho; Kim, H. J.; Senthil, K.; Prabakar, K. Ultrahigh Surface Area Biomass Derived 3D Hierarchical Porous Carbon Nanosheet Electrodes for High Energy Density Supercapacitors. *Carbon N. Y.* **2021**, *174*, 463−474.
(70) Gogotsi, Y.; Simon, P. True Performance Metrics in Electrochemical Energy Storage. *Science (80-.).* **2011**, *334* (November), 917−918.
(71) Chen, C.; Zhao, M.; Cai, Y.; Zhao, G.; Xie, Y.; Zhang, L.; Zhu, G.; Pan, L. Scalable Synthesis of Strutted Nitrogen Doped Hierarchical Porous Carbon Nanosheets for Supercapacitors with Both High Gravimetric and Volumetric Performances. *Carbon N. Y.* **2021**, *179*, 458−468.
(72) Sangtong, N.; Chaisuwan, T.; Wongkasemjit, S.; Ishida, H.; Redpradit, W.; Seneesrisakul, K.; Thubsuang, U. Ultrahigh-Surface-Area Activated Biocarbon Based on Biomass Residue as a Supercapacitor Electrode Material: Tuning Pore Structure Using Alkalis with Different Atom Sizes. *Microporous Mesoporous Mater.* **2021**, *326* (June), 111383.
(73) Zheng, L. H.; Chen, M. H.; Liang, S. X.; Lü, Q. F. Oxygen-Rich Hierarchical Porous Carbon Derived from Biomass Waste-Kapok Flower for Supercapacitor Electrode. *Diam. Relat. Mater.* **2021**, *113* (January), 108267.
(74) Roy, C. K.; Shah, S. S.; Reaz, A. H.; Sultana, S.; Chowdhury, A. N.; Firoz, S. H.; Zahir, M. H.; Ahmed Qasem, M. A.; Aziz, M. A. Preparation of Hierarchical Porous Activated Carbon from Banana Leaves for High-Performance Supercapacitor: Effect of Type of Electrolytes on Performance. *Chem. - An Asian J.* **2021**, *16* (4), 296−308.
(75) Taer, E.; Natalia, K.; Apriwandi, A.; Taslim, R.; Agustino, A.; Farma, R. The Synthesis of Activated Carbon Nano Fiber Electrode Made from Acacia Leaves (Acacia Mangium Wild) as Supercapacitors. *Adv. Nat. Sci. Nanosci. Nanotechnol.* **2020**, *11* (2), 25007.
(76) Yao, Y.; Chen, X.; Yu, N.; Wei, F.; Feng, H. Preparation and Supercapacitive Performance of Lead Dioxide Electrodes with Three-Dimensional Porous Structure. *Russ. J. Electrochem.* **2018**, *54* (7), 585−591.

https://doi.org/10.1021/acsomega.2c04301
ACS Omega 2022, 7, 36489−36502